

Chapter 8

Ramp-rate limitation of dipole magnets

In this chapter the effect of interfilament-, interstrand- and boundary-induced coupling currents on the ramp-rate limitation (RRL) of the quench current in dipole magnets is investigated.

A significant reduction of the quench current as a function of the field-sweep rate can be observed in magnets with a large as well as a small contact resistance between crossing strands.

The RRL in magnets with small contact resistances is shown to be mainly related to the power loss, generated in the contact resistances, especially in coils with poorly cooled conductors. In this case, the RRL of the magnet can be used to estimate the thermal conductivity of the cable insulation.

The RRL in magnets with large contact resistances is shown to be mainly attributed to the presence of boundary-induced coupling currents. The magnitude of these coupling currents can be influenced by performing field precycles (before the actual ramp to quench).

The results of the RRL of a few 1 and 10 m long LHC dipole model magnets are evaluated. The temperature of the cable is calculated as a function of the average coupling power loss assuming a uniform contact resistance over the cross-section of the coils and uniform temperature within each turn of the magnet. It is shown that the temperature increase in the coil due to beam losses can be well estimated by a detailed analysis of the RRL.

8.1 Introduction

Accelerator dipole magnets are normally operated at a low central-field-sweep rate of the order of 10^{-2} Ts^{-1} . Higher field-sweep rates of up to 10^{-1} Ts^{-1} occur during a fast de-excitation in the case of a quench in one of the series-connected magnets. During a field sweep the temperature increase in the cable and the induced coupling currents should be as small as possible in order to ensure a good stability of the superconductor.

The effect of the coupling currents on the electromagnetic stability is investigated by means of the *Ramp-Rate Limitation (RRL)* of the quench current. Three types of coupling currents are dealt with in sections 8.2.1-8.2.3:

- The *Interfilament Coupling Currents (IFCCs)* which are induced within a strand subject to a varying magnetic field \dot{B} (see section 3.4).
- The *Interstrand Coupling Currents (ISCCs)* which are induced in and between the strands of a cable subject to a varying magnetic field \dot{B} (see chapter 4).
- The *Boundary-Induced Coupling Currents (BICCs)* which are generated due to spatial variations of \dot{B} (and, to a smaller extent, the cross-contact resistance R_c) along the cable length (see chapter 5). The BICCs strongly influence the current distribution among the strands of the cable and therefore the maximum transport current.

The temperature increase in the cable (during a field sweep) is investigated in section 8.2.4. It is assumed that the heat is generated by the IFCCs and ISCCs. The enhancement of the interstrand coupling power loss (ISCL) due to the BICCs is disregarded as well as the losses in the filaments, wedges, collars and yoke as they all are relatively small compared to the ISCL.

The reduction of the quench current as a function of the field-sweep rate is calculated for the PBD magnet as specified in Table 2.1. Experimentally obtained values for the time constants of the IFCCs and the cross-contact resistances of cables are used to obtain a first qualitative estimate of the RRL. It is shown that the main cause of the RRL can be deduced from the shape of the curve relating the quench current and the field-sweep rate.

In sections 8.3-8.5 the RRL is presented which is experimentally observed in several LHC dipole model magnets. The analysis of the RRL is focused on the following questions:

- Do the BICCs affect the temperature margin of the cable and what is the magnitude of the BICCs during ramping of the magnets?
- What is the expected increase of the cable temperature due to beam losses in the coils?
- What is the maximum allowable de-excitation rate of the magnets?

The methods described in this chapter and the experimental results show which possibilities the analysis of the RRL offers with respect to the understanding of the electrodynamics of superconducting magnets. Specific conclusions about the observed RRL in the LHC model magnets are difficult to draw. Firstly, because the RRL of only a few magnets is determined and secondly because the quench current is strongly affected by local variations in the coupling currents and power loss as well as variations of the local critical current density in the cable. Investigation of the RRL is therefore much more complicated than the analysis of the coupling loss (chapter 6) or the coupling-current induced field distortions (chapter 7) which both represent a more *average* effect over the coils.

8.2 Calculation of the RRL of magnets

In section 2.4 an empirical scaling law is presented that describes the relation between the critical current I_C of NbTi superconductors as a function of the applied field B and the temperature T [Lubell, '83]:

$$I_C = (C_1 - C_2 |B|) \left(1 - \frac{T}{T_C(B, I=0)} \right) \quad [\text{A}] \quad \text{for } |B| > B^*, \quad (8.1a)$$

with:

$$T_C(B, I=0) = 9.2(1 - |B|/14.5)^{0.59} \quad [\text{K}], \quad (8.1b)$$

where B^* is about 3 T. The relation for the critical current for $B < B^*$ is disregarded here since the treatment of the RRL is focused on high-field magnets with quench fields well above 3 T. Eqs. 8.1a and 8.1b can be rewritten for an arbitrary strand section in the cable of a coil:

$$I_{C, str} = (C_1 - C_2 |B_{str}|) \left(1 - \frac{T_{cab}}{9.2} \left(1 - |B_{str}|/14.5 \right)^{-0.59} \right) \quad [\text{A}] \quad \text{for } |B| > B^*, \quad (8.2)$$

with B_{str} the local field at the given strand section and T_{cab} the temperature of this strand section. The field B_{str} is composed of the field \mathbf{B}_{tr} produced by the transport current, and the field \mathbf{B}_{cc} caused by the ISCCs and the BICCs:

$$|B_{str}| = |\mathbf{B}_{tr} + \mathbf{B}_{cc}| = \beta_{str} T_M N_s I_{tr, str} + |B_{cc}| \operatorname{sgn}(\dot{B}_{ce}) \quad [\text{T}], \quad (8.3)$$

with T_M the field factor of the magnet and β_{str} the ratio between the local field (at the given strand position) and the central field (see Fig. 6.1). The vector summation is transformed into a scalar operation since the orientation of the fields \mathbf{B}_{tr} and \mathbf{B}_{cc} is basically in the y -direction for the blocks near the midplane where almost all quenches are located (see section 8.3).

The quench current $I_{q, str}$ of a strand is here defined by the maximum transport current $I_{tr, str, max}$ that a section of the strand can carry in the presence of additional coupling currents. Assuming that:

- the weakest strand determines the quench current of the entire magnet,
 - the transport current is uniformly distributed among the strands,
- the quench current of the magnet is defined by:

$$I_q = N_s I_{q, str} \quad [\text{A}], \quad (8.4)$$

and the quench field by:

$$B_q = T_M I_q \quad [\text{T}]. \quad (8.5)$$

The current $I_{q,0}$ and the field $B_{q,0}$ denote the quench current and quench field respectively if the coupling currents are zero.

The following assumptions are made:

- Ramp-rate-induced quenches are not initiated by a conductor movement or a transient energy pulse from the environment.
- The temperature T_{cab} of the cable does not vary over the cross-section of the cable and along the length of a given turn. The influence of the coil ends on the temperature distribution in the cable is not taken into account.
- The quench starts in the strand section in which the total current becomes equal to the critical current at the given field and temperature.
- A quench that occurs locally in a strand section causes a quench of the whole coil. Recovering of the quench due to, for example, redistribution of the strand currents after a quench is not taken into account.
- The cross-contact resistance R_c is constant over the whole cross-section of a coil.
- The resistive loss, generated in the cable-to-cable connections, the eddy current loss in the copper wedges and the collars and the magnetisation loss in the filaments and the iron yoke are disregarded. These loss contributions are relatively small at the field and field-sweep rate used in the quench experiments (see sections 8.3-8.5).
- The voltage over a strand is assumed to be 0 up to $I_{str}=I_{q, str}$. A variation of the coupling-current distribution at strong excitation (see section 4.5) is therefore disregarded.
- The transport current is uniformly distributed among the strands.

In sections 8.2.1-8.2.4 the influence of the various coupling currents and the coupling power loss on the quench current is presented. The discussion is illustrated by means of calculations of the RRL in a PBD magnet (see Table 2.1) using $C_1=1.12 \cdot 10^5$ A and $C_2=7.79 \cdot 10^3$ AT⁻¹ in eq. 8.2. Other values for the constants C_1 and C_2 give basically the same results if the quench currents are normalised to the maximum values $I_{q,0}$. A 26-strand cable is considered with a cross-section of $17 \times 2.04/2.50$ mm² and a cable pitch $L_{p,s}=0.13$ m. The reduction of the quench current is estimated for the anticipated average field-sweep rate of about 0.0066 Ts⁻¹ and initial field-sweep rate of -0.084 Ts⁻¹ in the case of a fast exponential de-excitation.

8.2.1 Influence of IFCCs on the RRL

In section 3.4 it is shown that the maximum transport current in a strand is affected by the IFCCs flowing in the outer layer of filaments, and can be expressed by:

$$I_{tr, str, max} = I_{C, str} \left(1 - \frac{(\pi d_s^*)^2 \tau_{if}}{I_{C, str} \mu_0 L_{p, f}} \left| \dot{B}_{str} \right| \right)^2 \quad [\text{A}], \quad (8.6)$$

with $I_{C, str}$ as defined by eq. 8.2 and $\dot{B}_a = \dot{B}_{str}$, by which the small twist angle of the cable is disregarded. The quench current is then given by the condition that the transport current is equal to the maximum transport current, so $I_{q, str} = I_{tr, str} = I_{tr, str, max}$, and is iteratively calculated by combining eqs. 8.2, 8.3 and 8.6.

As an example, the characteristic relative reduction of the quench current of the PBD magnet is depicted in Fig. 8.1 as a function of \dot{B}_{ce} for $L_{p, f}=25$ mm, $d_s^*=1.2$ mm, $T_b=1.9$ and 4.3 K and $\tau_{if}=50$ and 100 ms. The cable temperature is constant and equal to T_b .

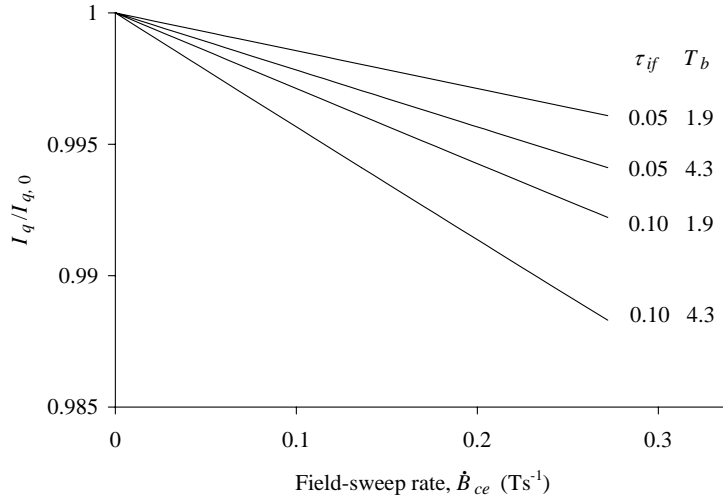


Figure 8.1. Calculation of the relative quench current of the PBD magnet caused by the IFCCs as a function of the central-field-sweep rate. Curves for two τ_{if} -values (in seconds) are depicted at bath temperatures of 1.9 K and 4.3 K.

The quench origin is located in block 6 near the aperture (at $r \approx 25$ mm, see Fig. 2.2a) since the local field and therefore also \dot{B}_{str} ($=\beta_{str} \dot{B}_{ce}$, see also Fig. 6.1) are maximum in this part. In the case of dipole magnets with other geometries or cables with other characteristics the reductions are different since parameters such as β_{str} , d_s^* , L_{pf} and τ_{if} are incorporated in eqs. 8.2 and 8.6. The RRL due to the presence of IFCCs can be easily calculated for any magnet geometry if τ_{if} is known. Fig. 8.1 shows that the reduction is a factor 1.5 larger at 4.3 K than at 1.9 K.

The reduction of the quench current of the LHC dipoles at $\dot{B}_{ce}=0.0066$ Ts⁻¹ will be smaller than 0.01% (for $\tau_{if}=0.05$ s) whereas at fast de-excitation ($\dot{B}_{ce}=-0.084$ Ts⁻¹) it is still smaller than 0.1%. Only for magnets which are subject to very large field-sweep rates, does the reduction of the quench current due to the IFCCs have to be taken into account.

8.2.2 Influence of ISCCs on the RRL

It is shown in section 4.4.1 that the ISCCs in Rutherford-type cables are mainly created by a field change \dot{B}_\perp normal to the cable width (see Fig. 4.1). Here the case of a positive field-sweep rate is dealt with (see section 8.5 for negative field-sweep rates). The critical part of the coil with respect to the quench current is near the aperture, in the strand sections that bend around the edge of the cable, because:

- fields B_{tr} and B_{cc} are maximum,
- the ISCCs flow in the same direction as the transport current and are maximum (see eqs. 7.11 with $x=w/N_s$).

According to eq. 7.11, the maximum ISCC in turn i at the edge of the cable can be expressed by:

$$I_{s,i,max} = 0.0415 \frac{L_{p,s} w N_s}{R_{c,i}} \beta_{I,i} \dot{B}_{ce} \cos(\pi / N_s) \quad [\text{A}], \quad (8.7)$$

with $\beta_{I,i}$ the field geometry factor that depends on the magnitude and the shape of the field variation $\dot{B}_{\perp c}$ across the cable width of turn i (see Fig. 7.2).

The quench current in a strand section:

$$I_{q,str} = I_{C,str} - I_{s,max} \quad [\text{A}], \quad (8.8)$$

is calculated iteratively using $I_{tr,str} = I_{q,str}$ in eq. 8.3. The quench origin will depend on \dot{B}_{ce} since $I_{q,str}$ depends on β_{str} and β_I which both vary over the cross-section of the coils.

The relative reduction of the quench current of the PBD magnet is depicted in Fig. 8.2 for R_c -values of 1, 2 and 5 $\mu\Omega$ and bath temperatures of 1.9 K and 4.3 K. If \dot{B}_{ce} is small then the ISCCs are also small and the quench starts in block 6 where β_{str} is maximum (and hence $I_{C,str}$ is minimum). The ISCCs become larger for increasing \dot{B}_{ce} and the quench origin shifts therefore to block 3 where β_I is maximum. Note that the relative quench reduction is a factor 1.5 larger at 4.3 K than at 1.9 K. In the case of cables with a different geometry, the RRL is proportional to $I_{s,max}$ and hence to $L_{p,s} w N_s / R_c$.

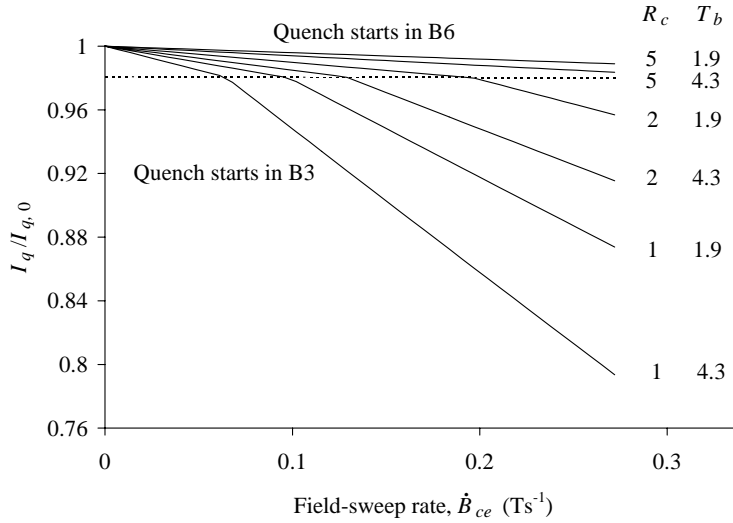


Figure 8.2. Calculation of the relative reduction of the quench current of the PBD magnet caused by the ISCCs as a function of the central-field-sweep rate. Curves for three different R_c -values (in $\mu\Omega$) are depicted at bath temperatures of 1.9 K and 4.3 K. The dotted line illustrates the two different quench origins.

The reduction of the quench current of the LHC dipole magnets at $\dot{B}_{ce} = 0.0066 \text{ Ts}^{-1}$ will be smaller than 0.15% (for $R_c = 1 \mu\Omega$). At fast de-excitation, there is no reduction because the transport current and the ISCC have opposite sign near the aperture where the field is maximum (see section 8.5).

8.2.3 Influence of BICCs on the RRL

In chapters 5 and 7 it has been shown that the BICCs exhibit large characteristic times τ_{bi} and that their magnitude is proportional to \dot{B}_{ce} . Therefore, the magnitude of the BICCs at the moment of the quench depends not only on \dot{B}_{ce} but also on the time t_r of the ramp. This large characteristic time results in a different evaluation of the RRL caused by the BICCs compared to the ISCCs, for which $\tau_{is} \ll t_r$. The BICCs during the ramp can be expressed by (assuming that their magnitude is equal to 0 at $t=0$):

$$I_{bi} = C_{bi} \dot{B}_{ce} (1 - e^{-t/\tau_{bi}}) \quad [\text{A}], \quad (8.9)$$

with t the time from the beginning of the ramp and C_{bi} a constant with dimension AsT^{-1} . Note that this exponential expression for the BICCs does not describe their real time-dependent behaviour as discussed in sections 5.4.1-5.4.4. It is, however, the most practical approximation by which the effect of the BICCs on the RRL can be investigated. The constant C_{bi} is rather unpredictable since it is determined by the integral effect of many BICCs induced by the numerous \dot{B}_{\perp} -variations along the cable in the coil. The order of magnitude of C_{bi} can be estimated by calculating the magnitude of the BICCs (using eq. 5.5) due to the variation of \dot{B}_{\perp} in one turn of the coil. This would give a C_{bi} of about $5 \cdot 10^3 \text{ AsT}^{-1}$ for a PBD magnet with $\xi=1 \text{ m}$ (as estimated at the end of section 7.7.5) and $R_c=3 \mu\Omega$.

Fig. 8.3 illustrates the calculated current I_{bi} during a linear ramp from $I_{tr,str}=0$ to 500 A at small and large ramp rates ($\dot{I}_{tr,str}=1$ and 10 As^{-1}) with $\tau_{bi}=100 \text{ s}$ and $\tau_{is}=4 \text{ s}$. The steady-state magnitude of the BICC is a factor 5 larger than that of the ISCC. Note that for a large ramp rate the BICC has not yet achieved its steady-state value at the end of the ramp. It is assumed that the strand quenches if the total strand current I_{str} exceeds 500 A. Comparing both figures it is clear that the reduction of the quench current (i.e. the maximum transport current) will no longer be proportional to the ramp rate as in the case of the IFCCs and the ISCCs.

The quench current in a given strand section in the presence of BICCs:

$$I_{q,str} = I_{C,str} - I_{bi} \quad [\text{A}], \quad (8.10)$$

is iteratively calculated by using $I_{q,str}=I_{tr,str}$ in eq. 8.3. The typical shape of the $I_{q,str}-\dot{B}_{ce}$ curve is depicted in Fig. 8.4 in the case of the PBD magnet with $C_{bi}=5 \cdot 10^3, 1 \cdot 10^4$ and $2 \cdot 10^4 \text{ AsT}^{-1}$, $\tau_{bi}=100$ and 200 s and for an initial transport current of 0 A.

The quench current decreases rapidly for small \dot{B}_{ce} , whereas the reduction becomes milder for large \dot{B}_{ce} . The initial slope of the curve is related to C_{bi} and is independent of τ_{bi} . The shape of the curve is related to C_{bi} as well as τ_{bi} . The initial slope is a factor 1.5 larger at 4.3 K than at 1.9 K, which is similar to the case of the reduction due to the IFCCs and the ISCCs.

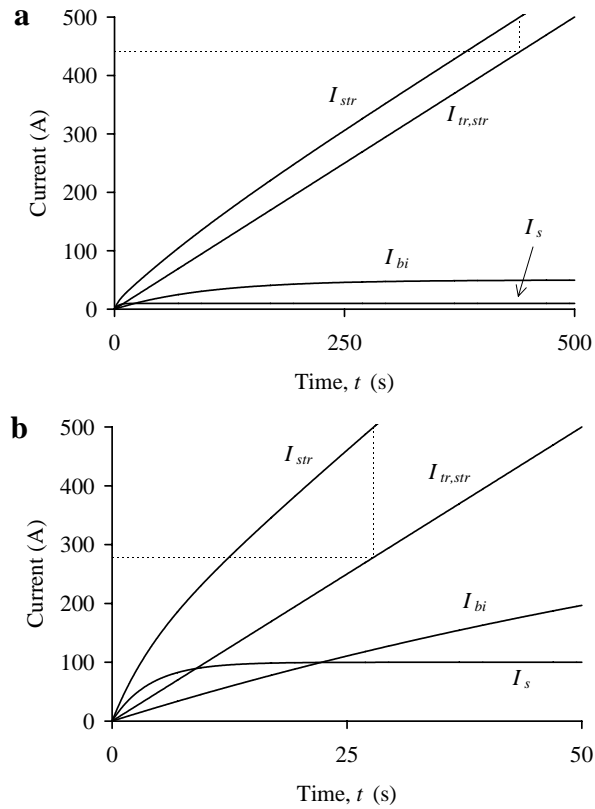


Figure 8.3.

Simulation of the three current contributions $I_{tr,str}$, I_s and I_{bi} to the total strand current I_{str} during a linear ramp with:

- a. a small ramp rate,
- b. a large ramp rate.

The ISCC (with $\tau_{is}=4$ s) and the BICC (with $\tau_{bi}=100$ s) are assumed to be 0 at $t=0$. The dotted lines show the transport current at which the strand current is equal to 500 A.

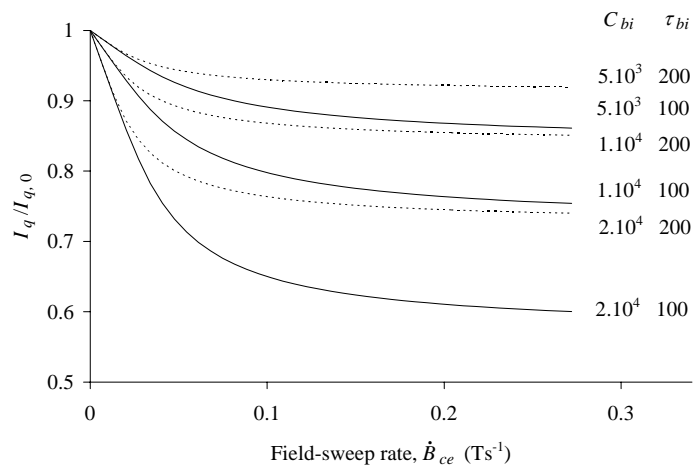


Figure 8.4. Calculation of the relative reduction of the quench current of the PBD magnet caused by the BICCs as a function of the central-field-sweep rate. Curves for three different C_{bi} -values (in AsT^{-1}) are depicted for $\tau_{bi}=100$ (normal lines) and 200 s (dotted lines), $T_b=1.9$ K.

The reduction is influenced by the excitation history of the magnet if the BICCs, that are induced during the preceding sweeps, are not yet negligible. As a working rule, any field sweep that is performed in the past and not longer ago than a few times τ_{bi} , can increase as well as decrease the RRL. In general, preceding field sweeps with a positive (negative) sign increase (reduce) the RRL.

An illustration is given in Fig. 8.5 where the ramps shown in Fig. 8.3 are preceded by a field sweep with negative ramp rate. Comparing Figs. 8.3 and 8.5, it is clear that the quench current is significantly *larger* if the preceding ramp has opposite sign and the time of the final ramp is comparable or smaller than τ_{bi} .

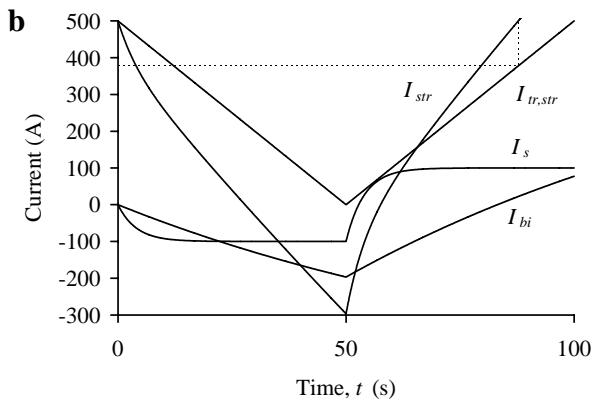
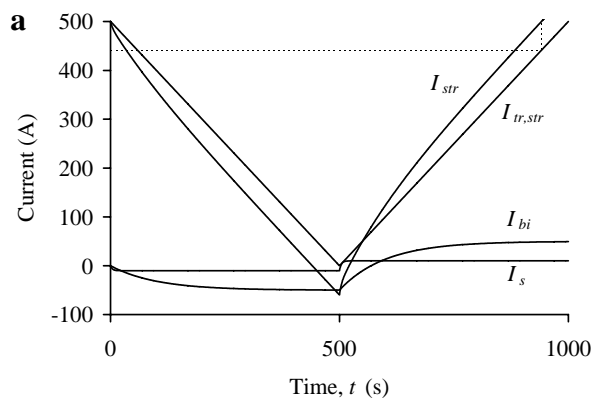


Figure 8.5.

Simulation of the three contributions $I_{tr,str}$, I_s and I_{bi} to the total strand current I_{str} during a cycle of $I_{tr,str}$ of 500-0-500 A, with:

- a: a small ramp rate,
- b: a large ramp rate.

The ISCC (with $\tau_{is}=4$ s) and the BICC (with $\tau_{bi}=100$ s) are assumed to be 0 at $t=0$. The dotted lines show the transport current at which the strand current is equal to 500 A.

This increase in the quench current due to a partial compensation of the BICCs is further investigated in the case of a PBD magnet for several values of τ_{bi} and C_{bi} . The conditions are the same as used in Fig. 8.4 but now the ramp-to-quench is preceded by a ramp from $I_{q,0}$ to 0 A (see Fig. 8.6).

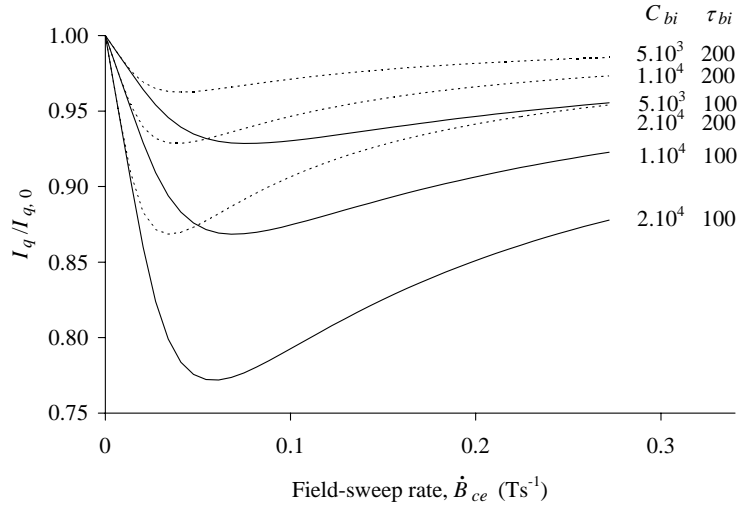


Figure 8.6. Calculation of the relative reduction of the quench current of the PBD magnet caused by the BICCs as a function of the central-field-sweep rate. Curves for three different C_{bi} -values (in AsT^{-1}) are depicted for $\tau_{bi}=100$ (normal lines) and 200 s (dotted lines), $T_b=1.9$ K. The ramp to quench is preceded by a ramp from $I_{q,0}$ to 0.

The ratio $I_q/I_{q,0}$ attains a minimum which depends on C_{bi} as well as τ_{bi} . The slopes of the curves for $\dot{B}_{ce} \rightarrow 0$ are independent of τ_{bi} and are the same as those of Fig. 8.4 (for quenches without a precycle), because the time of the ramp is much larger than τ_{bi} so that the BICCs approach their steady-state values before the end of the ramp. In the case of larger field-sweep rates the difference in the quench currents with and without precycles increases steadily as can be seen easily from Figs. 8.4 and 8.6 (see also section 8.2.5).

8.2.4 Influence of ISCL on the RRL

In section 4.4.1 it is shown that the ISCL in Rutherford-type cables is mainly generated in the contact resistances R_c caused by a field change normal to the cable width. The ISCL (per metre of cable) depends on the time t from the start of the ramp, and can be expressed by (for a uniform \dot{B}_\perp):

$$P_c = 8.5 \cdot 10^{-3} \frac{L_{p,s} w^2 (N_s^2 - N_s)}{R_c} \dot{B}_\perp^2 (1 - e^{-t/\tau_{is}})^2 \quad [\text{Wm}^{-1}]. \quad (8.11)$$

Eq. 8.11 leads to the power density in turn i of a coil as a function of \dot{B}_{ce} :

$$P_{c,i} = 8.5 \cdot 10^{-3} \frac{L_{p,s} w (N_s^2 - N_s)}{h R_{c,i}} \beta_{p,i}^2 \dot{B}_{ce}^2 (1 - e^{-t/\tau_{is,i}})^2 \quad [\text{Wm}^{-3}], \quad (8.12)$$

with β_p the field geometry factor as given in Fig. 6.2. In the following, the $R_{c,i}$ and $\tau_{is,i}$ values are assumed to be the same in all the turns of the coil and equal to R_c and τ_{is} .

The enhancement of the ISCL due to the BICCs is disregarded here. The increase is estimated (see also section 5.5) to be much smaller than the ISCL due to the ISCCs. The periodic pattern of the local power loss (see Figs. 5.12 and 5.13) does not cause a significant spatial variation of the cable temperature within a turn because the thermal conductivity of copper (about $250 \text{ Wm}^{-1}\text{K}^{-1}$) is about four orders of magnitude larger than that of the cable insulation. Due to the good electrical contacts between the strands, also the heat transfer from strand to strand will be much better than that from the strand to the helium outside the cable. Hence, the difference between the average cable temperature and the helium bath temperature is at least one order of magnitude larger than the temperature differences between the strands. In the following all strands in a turn are assumed to have the same temperature, equal to the average cable temperature T_{cab} .

To what extent the ISCL will heat up the (strand of the) cable depends, besides the parameters used in eq. 8.12, also on the heat transfer from the cable to the helium. The main thermal barrier is formed by the cable insulation (see Fig. 2.8). The heat transfer through the kapton layers and the glass-fibre tape cannot be predicted theoretically but has been determined by the following two experiments carried out by CEA-Saclay and CERN.

1. The temperature T_{cab} of the cable is determined as a function of the generated heat in the cable. Instead of a NbTi Rutherford-type cable, a stainless steel bar is used in which the heat is uniformly generated by means of resistive dissipation. The temperature increase of the central conductor in a stack of five conductors is depicted in Fig. 8.7 (curve 1) for a bath temperature $T_b=1.9 \text{ K}$ [Meuris, '91/'93]. The increase of T_{cab} vs. the resistive power loss is small up to a power-loss density of about 7 mW/cm^3 , where T_{cab} reaches the lambda point T_λ , and increases strongly for larger power losses. It is concluded that a large part of the heat is transferred through the small faces of the conductor [Meuris '91].
2. A certain heat flux is passed transversely through a stack of insulated copper cable pieces of which one side is kept at a constant temperature T_0 . The measurements are performed in vacuum. The effective thermal conductivity λ_{ins} of the total insulation is determined from the temperature difference between both sides of the stack [Dauguet, '92]. The coefficient λ_{ins} increases linearly as a function of the temperature and is equal to about 0.006 and $0.010 \text{ Wm}^{-1}\text{K}^{-1}$ for T_0 equal to 1.8 and 4.2 K respectively. The relation $\lambda_{ins}(T_0)$ is used to estimate the increase in the cable temperature due to a uniform heat dissipation in the cable, assuming that the heat transport occurs only through the two small faces of the cable. The results are shown in Fig. 8.7 (curve 2).

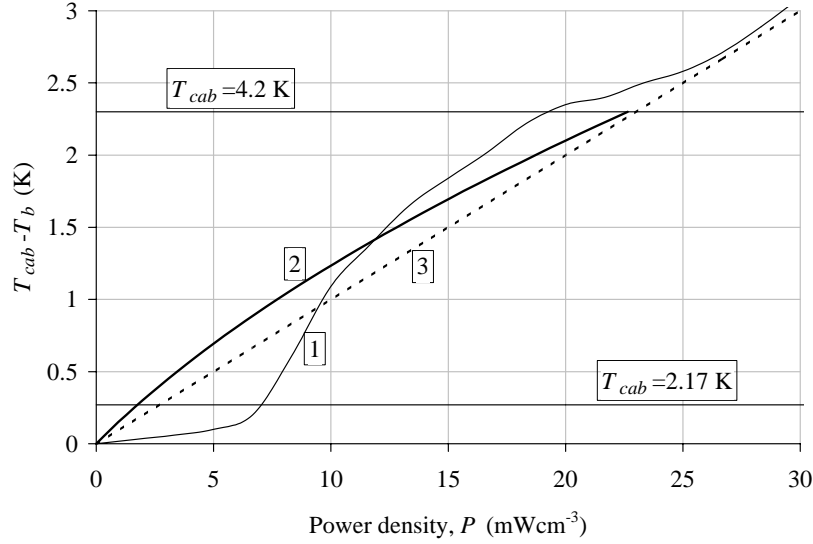


Figure 8.7. The temperature increase of a cable (at $T_b=1.9$ K) with an insulation as specified in Fig. 2.8 according to:
 1. [Meuris, '93],
 2. [Dauguet, '92], assuming that the heat is only transferred through the two small faces of the cable,
 3. eq. 8.10 with $q=10^4$ WK $^{-1}$ m $^{-3}$.

Note the initial small temperature increase of curve 1, for $T_{cab} < T_\lambda$, due to very high thermal conductivity of superfluid helium. It is beyond the scope of this thesis to treat the thermal behaviour of the cables in detail. However, in order to obtain representative values of the current reduction as a function of the ISCL, a simple linear approximation of the curves 1 and 2 is used, in the range of experimental interest, i.e. for power densities larger than 0.01 Wcm $^{-3}$ (see section 8.4). The cooling power is assumed to increase linearly with the temperature difference between the cable and the bath (see curve 3 in Fig. 8.7):

$$P_{cool} = q(T_{cab} - T_b) \quad [\text{Wm}^{-3}], \quad (8.13)$$

with q the effective thermal-conductivity coefficient per unit volume between the cable and the helium bath. A fit of eq. 8.13 to the experimental curves 1 and 2 shows that q is about 10^4 Wm $^{-3}$ K $^{-1}$ under steady-state conditions for $T_b=1.9$ K and $P > 0.01$ Wcm $^{-3}$. The linear approximation will be used to estimate the reduction of the quench current as a function of the dissipated power.

The temperature T_{cab} of turn i under steady-state conditions ($t \gg \tau_{is}$ and $P_c = P_{cool}$) is calculated by combining eqs. 8.12 and 8.13:

$$T_{cab,i} = T_b + 8.5 \cdot 10^{-3} \frac{L_{p,s} w (N_s^2 - N_s)}{h R_{c,i} q} \beta_{P,i}^2 \dot{B}_{ce}^2 \quad [\text{K}]. \quad (8.14)$$

The quench field is then determined by solving eq. 8.2 with T_{cab} as defined by eq. 8.14. In Fig. 8.8 the results are given of the calculated relative reduction of the quench current of the PBD magnet due to the ISCL, as a function of \dot{B}_{ce} , for constant q and steady-state conditions. Note that the reduction depends on the factor $(R_c q)$, so that the reduction for $R_c=1 \mu\Omega$ and $q=2 \cdot 10^4 \text{ Wm}^{-3}\text{K}^{-1}$ is identical to that for $R_c=2 \mu\Omega$ and $q=1 \cdot 10^4 \text{ Wm}^{-3}\text{K}^{-1}$.

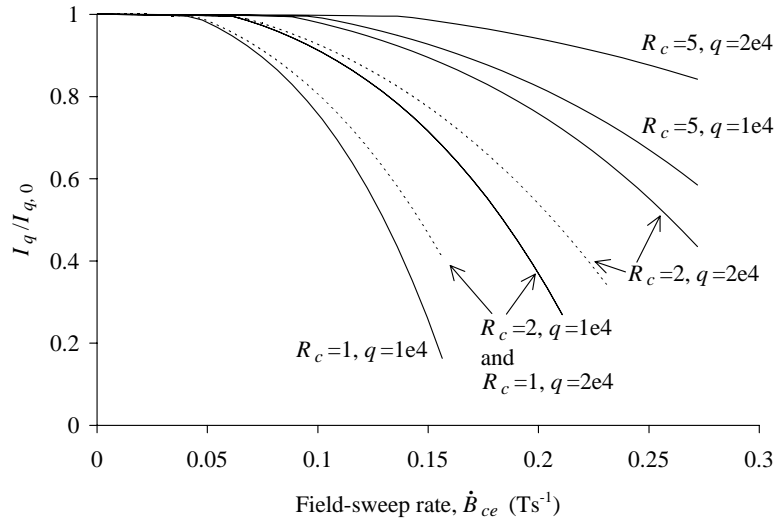


Figure 8.8. Calculation of the reduction of the relative quench current of the PBD magnet due to the ISCL as a function of the central-field-sweep rate. Various curves for different R_c (in $\mu\Omega$) and q (in $\text{Wm}^{-3}\text{K}^{-1}$) are shown for $T_b=1.9 \text{ K}$ and 4.3 K (dotted lines).

If \dot{B}_{ce} is small then the ISCL is also small and the quench starts in block 6 where β_{str} is maximum (and hence $I_{C,str}$ minimum). Should \dot{B}_{ce} be large then the ISCL also increases and the quench origin shifts to block 3 where β_p is maximum.

The generated coupling power loss causes a reduction of the quench current which is, in first approximation, linear with $\dot{B}_{ce}^2/(qR_c)$, and is larger at 4.3 K than at 1.9 K . Note that for increasing \dot{B}_{ce} the reduction of the quench current by temperature, due to the ISCL, is much larger than the reduction by over-current, due to the ISCCs, for the estimated cooling conditions and R_c -values between 1 and $10 \mu\Omega$.

8.2.5 Discussion

In practical dipole magnets the RRL is mainly caused by a combination of the IFCCs, the ISCCs, the BICCs and the ISCL. In section 8.2.1 it is shown that the reduction of the quench current due to the IFCCs is smaller than 0.1% for sweep rates up to 0.1 Ts^{-1} , and can be disregarded for the operation of accelerator dipole magnets. The quench current is then given by (assuming steady-state conditions):

$$I_{q,str}(B_{str}, \dot{B}_{ce}, T_{cab}) = I_{C,str}(B_{str}, T_{cab}) - I_{is}(\dot{B}_{ce}) - I_{bi}(\dot{B}_{ce}) \quad [\text{A}]. \quad (8.15)$$

The cooling conditions of the magnet, the heat capacity of the cable (and the helium in the voids of the cable), the field-sweep rate, the \dot{B}_\perp -distribution and the contact resistance are the main factors that determine which coupling currents or losses are the main cause of the RRL. Another important factor is the time scale of the field sweep as compared to the time constants τ_{is} and τ_{bi} . Since most of these parameters vary strongly over the cross-section of the coil and even along the length of a turn, it is impossible to calculate the RRL of a magnet accurately.

The dominant cause of the reduction can be deduced from the shape of the experimentally obtained I_q - \dot{B}_{ce} curve. The ISCCs initially cause a linear decrease (see Fig. 8.2), the BICCs a concave decrease (see Fig. 8.4) and the ISCL a convex decrease (see Fig. 8.8). In practice, however, it is probably a combination of the three causes that determines the RRL of a magnet. An example of a characteristic reduction of the quench current, caused by both the BICCs and the ISCL, is shown in Fig. 8.9 for the PBD magnet with $R_c=5 \mu\Omega$, $C_{bi}=10^4 \text{ AsT}^{-1}$, $q=10^4 \text{ Wm}^{-3}\text{K}^{-1}$ and $T_b=1.9 \text{ K}$.

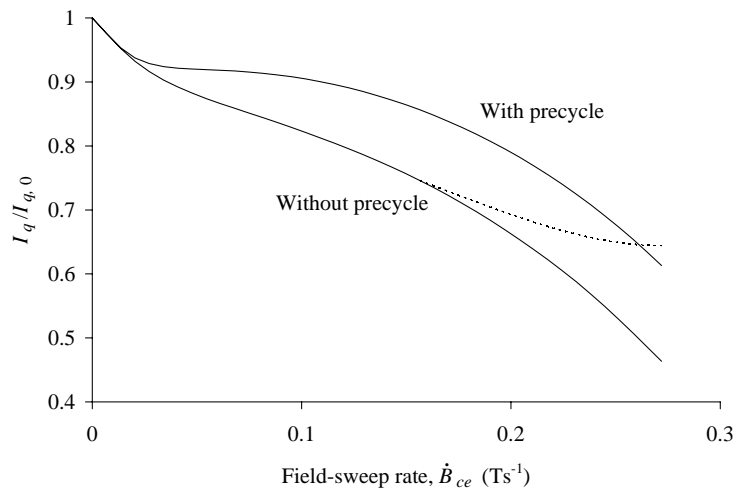


Figure 8.9. Calculation of the relative quench current due to a combination of the ISCL and the BICCs as a function of the field-sweep rate. The dotted line shows the milder decrease which occurs if the time of the ramp is too small to attain thermal equilibrium.

If \dot{B}_{ce} is small the reduction is caused by the BICCs, according to the initial slope of Figs. 8.4 and 8.6, whereas for a larger \dot{B}_{ce} the reduction is mainly caused by the ISCL. A precycle reduces the RRL for larger field-sweep rates. The shape of the curve changes if the ramp time t_r becomes too small to reach the steady-state conditions, that is thermal equilibrium. In this case the quench current will increase (see the dotted line) compared to the steady-state value. In the case of ramps with a precycle this increase is less pronounced because the ramp to quench is preceded by a ramp-down so that the total time to reach thermal equilibrium is much larger. For normal excitation of an accelerator magnet the RRL caused by the BICCs can be reduced by decreasing the field-sweep rate toward the end of the sweep (during a period of a few times τ_{bi}).

The difference in quench currents with and without a precycle is shown in Fig. 8.10. By presenting experimental quench results of a coil in this way, it is possible to estimate the magnitude of the BICC, that causes the quench, and its characteristic time. This approach is followed in section 8.3.

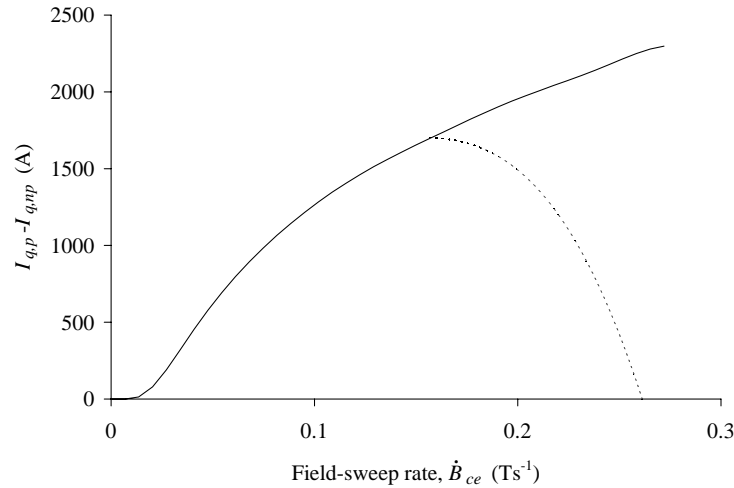


Figure 8.10. Calculation of the difference in the quench current between quenches with and without a precycle as a function of the field-sweep rate. The RRL is due to a combination of the ISCL and the BICCs. The dotted line shows the milder decrease which occurs if the time of the ramp is too small to reach thermal equilibrium.

The following points are important with respect to the stability and RRL of superconducting magnets, but a detailed evaluation falls beyond the scope of this thesis:

- In sections 8.2.1-8.2.4 it is assumed that the whole cable cross-section, i.e. all the strands, quenches if locally the current in a single strand exceeds the critical current. However, since the strands are in electrical contact with each other, the strand currents could redistribute as soon as some resistive voltage is built up over the strand. This leads to a decrease of the ISCCs whereas the total power loss remains the same (see section 4.5) so that the RRL could be less severe than calculated. A similar conclusion holds for the BICCs, of which the magnitude can also decrease once the total strand current approaches (or exceeds) the critical strand current. The process of redistribution probably depends strongly on the excitation level, the thermal properties of the cable and the characteristic times and magnitudes of the coupling currents.
- R_a and R_c also influence the temperature sharing between the strands and the heat transport between the strands and the helium. Hence, it can affect the sensitivity of the coil in the case of small transient heat pulses.
- The presence of coupling currents and ISCL always reduces the temperature margin of the coil for positive \dot{B}_{ce} . Small transient heat pulses which would not lead to a quench under DC conditions could, therefore, provoke a quench while ramping the magnet. This stability effect should be considered carefully when designing a magnet, by estimating the decrease of the temperature margin caused by the coupling currents and

the power loss, especially of magnets for which the field-sweep rate is fixed. In accelerator magnets the field-sweep rate can be reduced near the end of the excitation where the temperature margin is small. A decrease in the initial field-sweep rate in the case of a fast de-excitation is not possible.

- A non-uniform current distribution due to different joint resistances (see section 5.2) further decreases the temperature margin of the coil.
- The quench current, or the temperature margin, as a function of the field-sweep rate has to be estimated taking the smallest R_a and R_c and the worst cooling conditions that are expected to be present in the coil. Variations in the ISCL and the cooling conditions over small lengths (several cm) of the cable do not have to be taken into account since the high thermal conductivity of the cable results in a levelling of the cable temperature. Often these points are closely related and several authors have dealt with these stability effects, recently for example [Amemiya, '94], [Lvovsky, '95], [Ono, '95], [Vysotsky, '95a].

It is clear that the analysis of the RRL of magnets, in terms of the various coupling currents, power losses and cooling conditions, is very complicated. Although it is possible to clarify the mechanisms, it is difficult to extract specific conclusions. However, even rough estimates of the following topics are very interesting in order to optimise the performance of superconducting magnets:

- The influence of BICCs on the RRL, and in particular for the expected field-sweep rates during operation.
- The temperature increase of the cable as a function of the dissipation in the coils. This leads to an estimate of the required temperature margin in the case of beam losses in the coils.
- The RRL in the case of a fast de-excitation of the magnet.

These aspects will be evaluated in the subsequent three sections for the LHC dipole model magnets. The analysis is based on a limited number of quenches, performed on a few magnets. Nevertheless, the experimental results clearly demonstrate the basic mechanisms determining the quench behaviour of magnets during a field sweep.

8.3 Influence of BICCs on the RRL in LHC dipole magnets

The RRL of the LHC dipole model magnets is investigated by means of two different current sequences:

Quenches without a precycle (see Fig. 8.11a). The transport current is:

- ramped up from 0 to I_1 with a small field-sweep rate,
- kept constant for a time t_1 equal to 600 s,
- ramped up from I_1 to the quench current $I_{q,np}$ with a constant ramp rate.

Quenches with a precycle (see Fig. 8.11b). The transport current is:

- ramped up from 0 to I_1 with a small field-sweep rate,
- kept constant for a time t_1 equal to 600 s,
- ramped down from I_1 to I_2 with a constant ramp rate,
- kept constant for a time t_2 ,
- ramped up from I_2 to the quench current $I_{q,p}$ with a constant ramp rate.

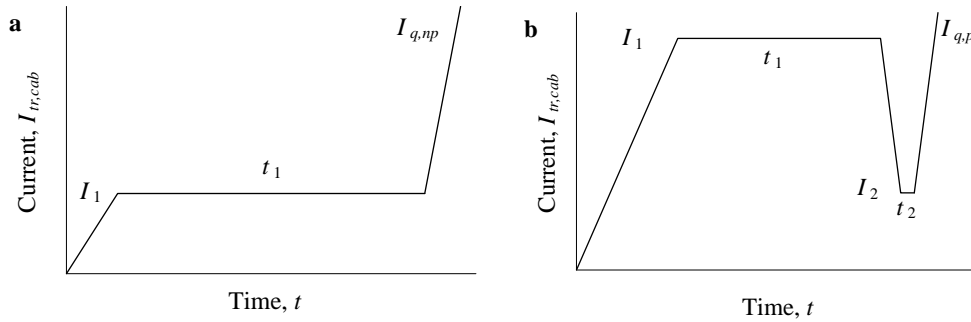


Figure 8.11. Current sequences for performing quenches **a.** without and **b.** with a precycle.

The waiting time t_1 of 600 s is chosen in order to stabilise the cable temperature and reduce the magnitude of the BICCs, which are observed to exhibit a characteristic time of about 10^2 s (see sections 7.7.1-7.7.5). The influence of the waiting time t_2 on the RRL can reveal the time constant τ_{bi} . The quench current will be maximum if t_2 is equal to 0 and will decrease, in first approximation, exponentially to the minimum value $I_{q,np}$ for $t_2 \gg \tau_{bi}$.

In the case of quenches with precycle, the current I_1 is chosen close to the expected quench current $I_{q,p}$ (usually within 500 A).

The reproducibility of the quench current is about 100 A for identical bath temperature and current history. Figs. 8.12 and 8.13 show the relative quench current as a function of \dot{B}_{ce} for quenches without precycle at $T_b=1.8$ -2.0 K and $T_b=4.3$ K respectively.

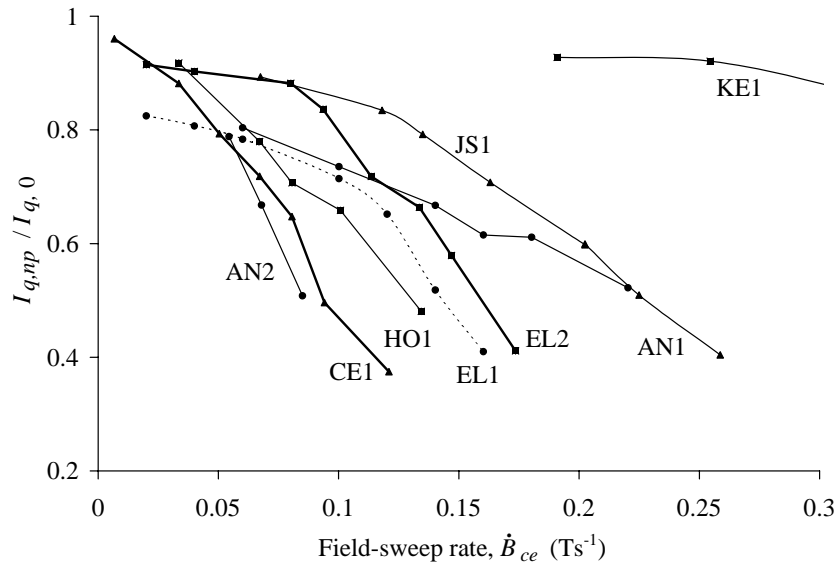


Figure 8.12. The relative quench current as a function of the central-field-sweep rate for quenches without precycle at $T_b=1.8$ -2.0 K and $I_1=3$ kA for several magnets as specified in Table 2.3.

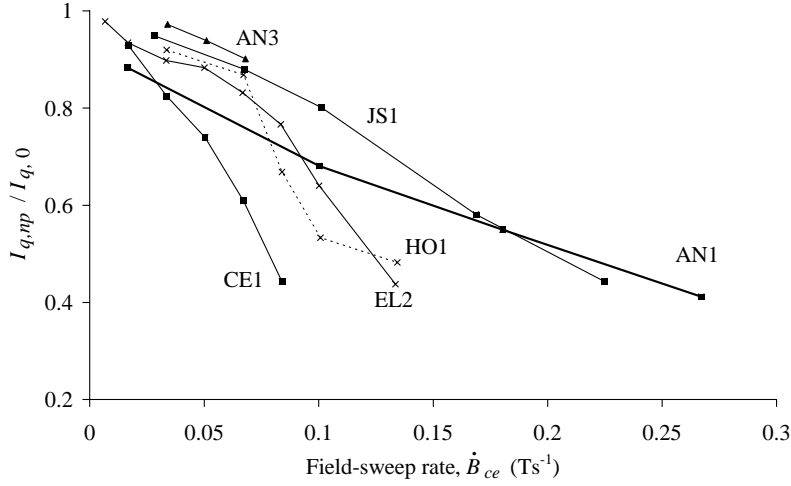


Figure 8.13. The relative quench current as a function of the central-field-sweep rate for quenches without precycle at $T_b=4.3$ K and $I_1=3$ kA for several magnets as specified in Table 2.3.

Ramp-rate-induced quenches at $T_b=1.8$ - 2.0 K and $\dot{B}_{ce}<0.02$ Ts⁻¹ could often not be performed since the training curve was not completed so that the quench current was not initiated by the coupling currents or the ISCL.

The quench currents are scaled to the measured quench current $I_{q,0}$ at $\dot{B}_{ce}=0.001$ Ts⁻¹. The average $I_{q,0}$ for the magnets is about 11500 A at 4.3 K and 15000 A at 1.9 K (N.B.: the $I_{q,0}$ -values for the KE1 magnet, made from a cable with a smaller cross-section, are about 14% smaller). If the training curve at 1.9 K is not completed, the current $I_{q,0}$ is estimated from the quench current at 4.3 K multiplied by the empirical factor 1.3 observed on a few magnets [Walckiers, '93]. Due to a possible error in $I_{q,0}$ it is not certain whether all the curves at 1.9 K are properly scaled. Hence, the strong reduction in the quench current for $\dot{B}_{ce}<0.05$ Ts⁻¹, especially for the EL1 magnet, can be caused by the BICCs (see Fig. 8.9) but can also be inherent to the scaling. At 4.3 K the initial reduction in $I_{q,np}$ is very likely to be attributed to the BICCs since $I_{q,0}$ is experimentally well determined.

The origins of almost all ramp-rate-induced quenches are located (by means of pick-up coils in the aperture of the magnets, see [Leroy, '93b], [Siemko, '95]) in the blocks 3 and 4 (see Fig. 2.2b) [Siemko, '94]. However, the quenches of each curve are not always located in the same aperture and the same quadrant.

The reduction of the quench current is about 20-80% larger at 4.3 K than at 1.9 K for large \dot{B}_{ce} . Since the calculated difference is about 50% (see section 8.2.4), this implies that the heat transfer (or cooling) is about the same at $T_b=1.9$ K and $T_b=4.3$ K (for large \dot{B}_{ce}). The thermal transfer between the cable and the helium is discussed in more detail in section 8.4.

The shapes of the curves show that the RRL is mainly affected by the ISCL for $\dot{B}_{ce}>0.05$ Ts⁻¹. Due to the apparent sharp reduction at small \dot{B}_{ce} , the BICCs have probably also a large effect (see Fig. 8.4). However, since the scaling can be quite inaccurate it is preferable to investigate the presence of BICCs by performing quench experiments after a

current precycle. The increase in the quench current if the ramp-up is preceded by a ramp-down (with $t_2=0$ s, see Fig. 8.11b) is shown in Fig. 8.14 for two magnets at $T_b=4.3$ K.

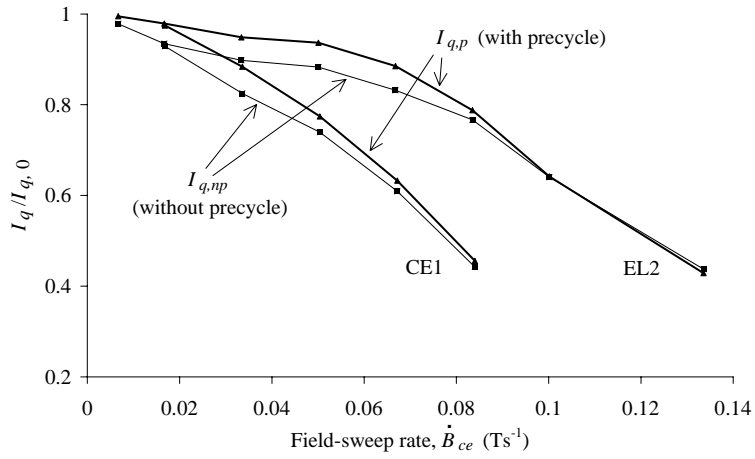


Figure 8.14. The quench currents, with and without a precycle, of the CE1 and EL2 magnets as functions of the central-field-sweep rate ($T_b=4.3$ K, $I_2=0$, $t_2=0$ s).

It can be clearly seen that the quench current with a precycle is much larger than without, especially for intermediate field-sweep rates, due to the partial compensation of the BICCs. The difference in quench currents ($I_{q,p}-I_{q,np}$) at $T_b=1.9$ K and 4.3 K is depicted in Figs. 8.15 and 8.16 respectively.

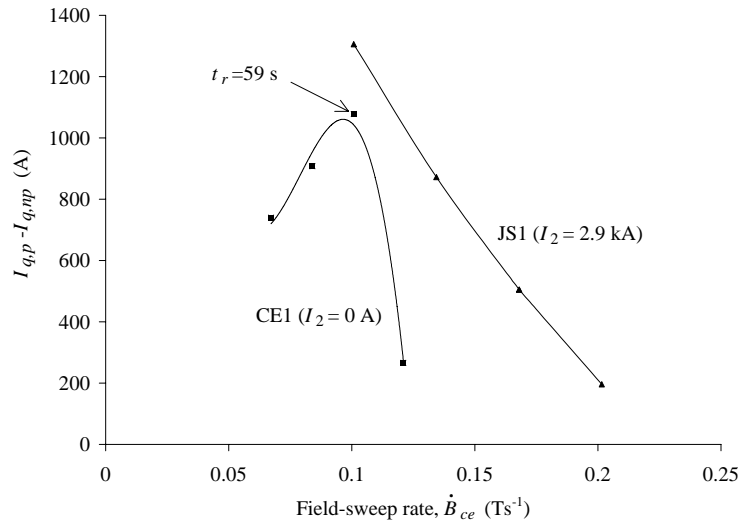


Figure 8.15. The difference in quench currents performed with and without a precycle as a function of the central-field-sweep rate at $T_b=1.8-2.0$ K ($t_2=0$, $I_{q,0}\approx 15$ kA). The labels indicate the ramp time t_r for maximum difference ($I_{q,p}-I_{q,np}$).

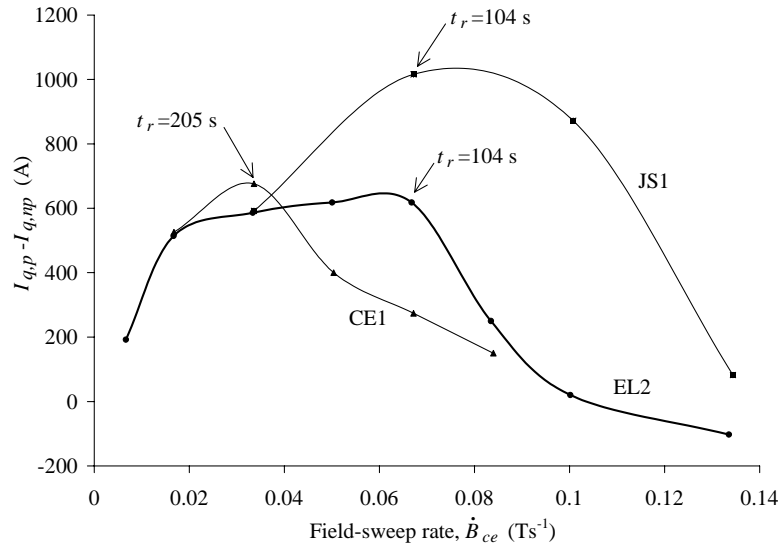


Figure 8.16. The difference in quench currents performed with and without a precycle as a function of the central-field-sweep rate at $T_b=4.3$ K ($I_2=0$, $t_2=0$, $I_{q,0}\approx 11.5$ kA). The labels indicate the ramp time t_r for maximum difference ($I_{q,p}-I_{q,np}$).

The figures show that a precycle causes an increase in the quench current up to a maximum of about 1000 A. This corresponds to the expected curves shown in Fig. 8.10 (note that the differences at small \dot{B}_{ce} could not be determined). The differences become smaller at larger field-sweep rates i.e. at ramp times t_r smaller than about 50-200 s, and they can even become negative as observed on the EL2 magnet. The most plausible explanation for the shape of the curves is that the temperature of the cable is not yet stabilised for the quenches without a precycle as shown in Fig. 8.10. The maximum of the curves for the CE1 magnet occurs at a smaller ramp time at $T_b=1.9$ K than at $T_b=4.3$ K, which suggests that the time required for temperature stabilisation is larger for the quenches at 4.3 K, probably caused by the different thermal properties of the helium or the larger heat capacity of the cable at 4.3 K.

The rising parts of the curves are used to estimate the magnitude of the BICCs, by fitting the simulations, which are presented in section 8.2.3, to the curves. Values for C_{bi} are found between $2\cdot 10^3$ to $5\cdot 10^3$ AsT⁻¹ and correspond well with the rough estimate of C_{bi} as made at the beginning of section 8.2.3. According to eq. 8.9, this implies that during excitation of the LHC dipoles with 0.0066 Ts⁻¹, BICCs will flow in the strands with steady-state values of up to 30 A, which is about as large as the transport current in the strands at injection ($I_{tr,str}\approx 35$ A) and about 7% of the transport current at nominal field ($I_{tr,str}\approx 470$ A). At fast de-excitation the BICCs can even attain values of about 400 A. However, due to the large characteristic time, the BICCs at the start of the de-excitation, where the current margin is still small, are much weaker (see also section 8.5).

The enhancement of the quench current due to a precycle will reduce if the time t_2 (see Fig. 8.11) between the precycle and the sweep to quench is large compared to the characteristic time τ_{bi} of the BICCs. The difference in quench currents ($I_{q,p} - I_{q,np}$) between quenches with and without a precycle should therefore have a maximum for $t_2 = 0$ and decrease towards 0 for $t_2 \rightarrow \infty$. The characteristic time of the decrease is, in first approximation, equal to τ_{bi} .

The effect of the waiting time t_2 on the quench current at $T_b = 1.9$ and 4.3 K is shown in Figs. 8.17 and 8.18. The quenches have only been incidentally performed on a few magnets. A very systematic analysis of the results is therefore not possible.

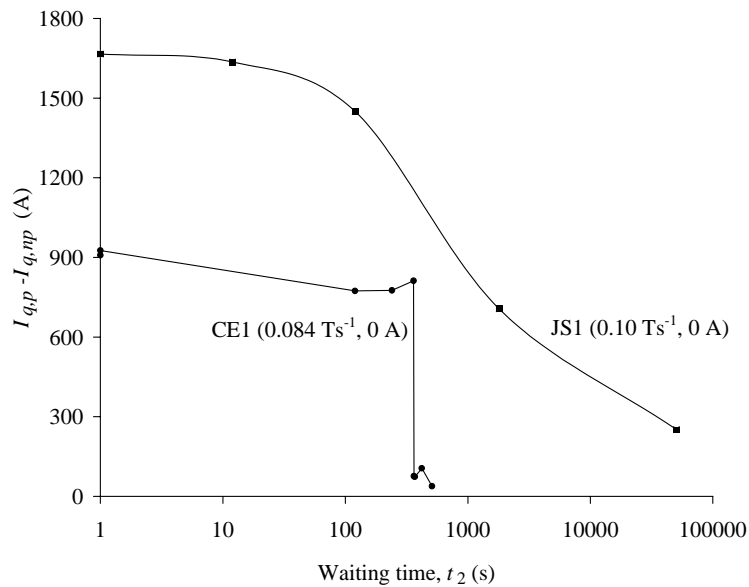


Figure 8.17. The difference in quench currents performed with and without a precycle as a function of the waiting time t_2 at $T_b = 1.9$ K. The labels indicate the central-field-sweep rate and the current I_2 .

The reduction of the quench current for increasing t_2 is clearly visible for all magnets except the EL2 magnet (for $I_2 = 5$ kA). Two types of curves are observed:

- curves for which $I_{q,p}$ gradually decreases with characteristic times of the order of 10^3 s,
- curves for which $I_{q,np}$ shows a peculiar sharp ‘step’ with a ‘width’ of less than 10 s.

The gradually decreasing curves correspond to expectations. The large characteristic time is probably caused by the spectrum of characteristic times that is present in a coil. In chapter 5 it is shown that τ_{bi} depends not only on the cable geometry but also on the effective strand resistivity and on the contact resistance. In a coil, each BICC exhibits a different characteristic time which usually increases if the average magnitude of the BICCs increases.

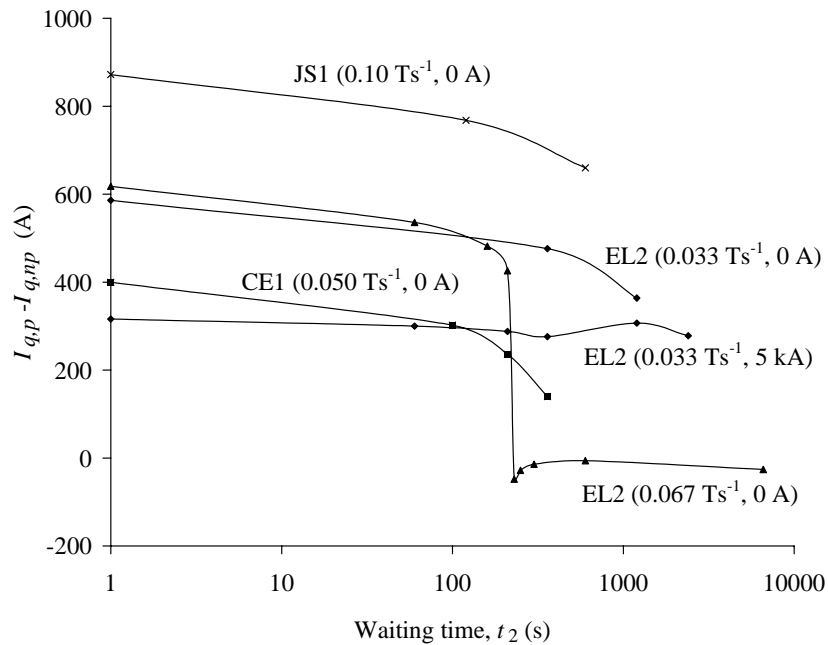


Figure 8.18. The difference in quench currents performed with and without a precycle as a function of the waiting time t_2 for $T_b=4.3$ K. The labels indicate the central-field-sweep rate and the current I_2 .

Since the quench is likely to be caused by large BICCs, the characteristic time deduced from Figs. 8.17 and 8.18 could be much larger than the average characteristic time as given in sections 7.7.1 and 7.7.3.

The reason of the peculiar ‘step’ in two $I_{q,p}-t_2$ curves is not understood. The quench values on the ‘left’ and ‘right’ sides of the step are very reproducible but the origins of the quenches on both sides of the step are different. During the waiting time t_2 there is no anomalous signal on any of the pick-up coils. A sudden current redistribution during t_2 is therefore probably not present. The most plausible explanation is that, during the ramp-up, part of (a strand of) the cable becomes normal which causes a quench on the right side of the step but recovers on the left. Field measurements (with a high sampling rate) during the ramp-up could perhaps reveal the exact reason.

This ‘step’ phenomenon could be related to the observed ramp-rate sensitivity on a CIC conductor where small sections of the cable seem to quench due to current loops in the cable [Vysotsky, ’95b]. In this conductor the quenches recover due to a fast redistribution of the current.

8.4 Estimate of the temperature increase of the cable due to power losses in the coil

In order to estimate the temperature of the cable due to the coupling loss, the $I_q-\dot{B}_{ce}$ curves have to be converted into $T_{cab}-P_c$ curves.

The field-sweep rate can be replaced by the estimated coupling-power density in the turn or block where the quench starts using eq. 8.12 assuming thermal equilibrium. Average R_c -values are used for this estimate, which are determined by means of the loss measurements and listed in Table 6.3.

The cable temperature just before the quench can be deduced from the quench current by combining eqs. 8.2, 8.3 and 8.14 assuming that $I_{bi}=0$. This assumption causes an error in the calculation of T_{cab} which is larger for quenches without a precycle than for quenches with a precycle. This is shown clearly in Fig. 8.19 where the $T_{cab}-P_c$ relation as deduced from the $I_q-\dot{B}_{ce}$ relation is shown in the case of the JS1 magnet at 1.9 and 4.3 K.

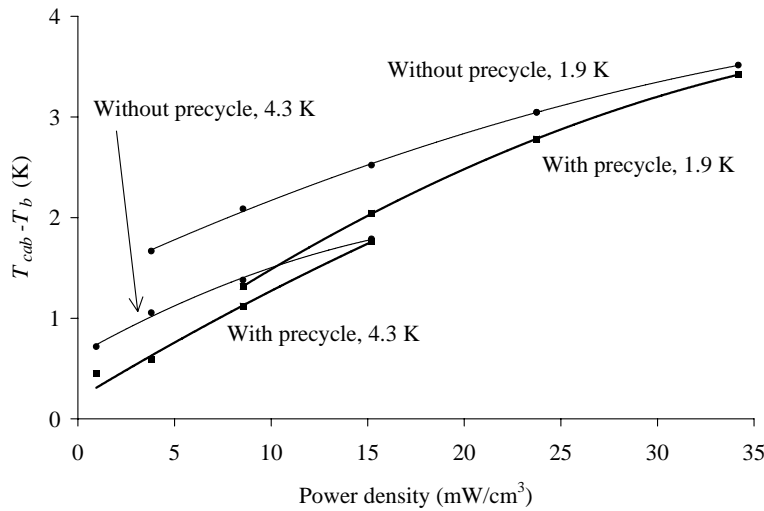


Figure 8.19. The estimate of the increase of the cable temperature caused by a steady-state heat dissipation in the cable of the JS1 magnet, deduced from the RRL with and without a precycle at $T_b=1.9$ and 4.3 K.

At 1.9 K, no quenches could be performed at small \dot{B}_{ce} , that is small P_c , because the training curve was not completed. Fig. 8.19 clearly shows that the conversion from a $I_q-\dot{B}_{ce}$ curve to a $T_{cab}-P_c$ curve results in relatively large errors if no precycle is performed, because it is obvious that $T_{cab}(\dot{B}_{ce} \rightarrow 0) = T_b$ if no BICCs are present. Extrapolation of the lower curves (deduced from the $I_{q,p}$ -values) supports this condition while extrapolation of the upper curves gives offset temperatures of about 1 K. Therefore, only the quenches with a precycle will give representative values for the temperature increase of the cable due to heat dissipation in the coil. The current of quenches performed without precycle can be strongly affected by the BICCs, which subsequently results in an overestimate of T_{cab} .

Quenches with a precycle have only been performed on a few magnets. Figs. 8.20 and 8.21 show the relations $T_{cab}-P_c$ as deduced from the quench currents at 1.9 and 4.3 K. A linear approximation according to eq. 8.13 is given as well.

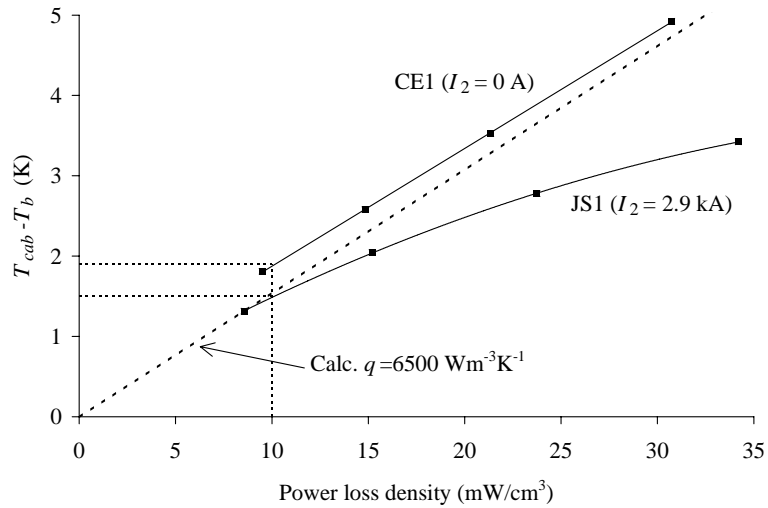


Figure 8.20. The estimate of the increase of the cable temperature due to a heat dissipation in the cable of the CE1 and JS1 magnets, deduced from the RRL with a precycle at $T_b = 1.9$ K ($t_2 = 0$). The linear dotted line shows the calculated relation using eq. 8.13 with $q = 6.5 \cdot 10^3$ Wm^3K^{-1} .

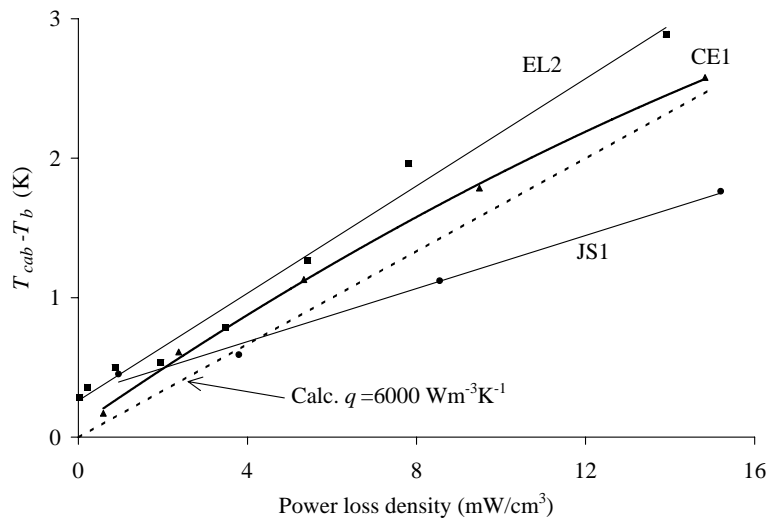


Figure 8.21. The estimate of the increase of the cable temperature due to a heat dissipation in the cable of the CE1, EL2 and JS1 magnets, deduced from the RRL with a precycle at $T_b = 4.3$ K ($I_2 = 0$, $t_2 = 0$). The linear dotted line shows the calculated relation using eq. 8.13 with $q = 6.0 \cdot 10^3$ Wm^3K^{-1} .

Fig. 8.20 shows that at $T_b=1.9$ K the cable temperature increases by about 1.5 K for a heat dissipation of 10 mW/cm^3 . The error is estimated to be smaller than 0.5 K and is mainly caused by:

- the use of an average R_c that is too large or too small compared to the local R_c in the turn where the quench starts, which results in a decrease, respectively increase, of the calculated power loss,
- additional BICCs in the cable, which results in an increase of the calculated cable temperature.

It is very encouraging that the temperature increase of about 1.5 K at $P_c=10 \text{ mW/cm}^3$ corresponds within 0.5 K to that deduced from the two experiments on small stacks of cable pieces (see Fig. 8.7). This proves not only that the temperature increase of a cable can be deduced by combining the electrical loss measurement and RRL of a coil, but also that the main mechanisms determining the RRL of magnets are well evaluated. Furthermore, the quantitative agreement between the various methods shows that the effective cooling surfaces of the cable in the coil itself and in a single stack are about the same (for power losses larger than $P_c=10 \text{ mW/cm}^3$), although the stress levels in a coil are much higher which could in fact reduce the size of the cooling channels considerably.

The evaluation of the temperature increase can be improved by supplying the turns in the coils, especially those near the midplane where the quenches start, with temperature sensors. The time required for thermal equilibrium of the cable can then be determined as well.

Quenches at a lower level of power losses can be induced at 4.3 K since the training sequence of the magnets is completed. A similar temperature increase is observed as at 1.9 K with a temperature increase between 1.3 and 2.3 K for $P_c=10 \text{ mW/cm}^3$. The difference in temperature increase at 1.9 and 4.3 K may be due to a different thermal conductivity or a different effective cooling surface. In the case of small power-loss densities, the curves deviate slightly from the expected linear decrease towards 0, caused by the BICCs which are not well compensated since the ramp time becomes large.

It is important that the coupling power loss can be directly related to the expected beam losses in the magnets since both types of losses are dissipated in the cables near the midplane of the magnet. Therefore, Fig. 8.20 shows directly the estimated temperature increase of the cable as a function of the beam losses in the coil windings. A precise estimate in the range between 0 and 10 mW/cm^3 , which is expected in the LHC magnets, is possible if the training sequence of the magnets is completed, which has unfortunately not been the case for the investigated magnets.

The accuracy of the method can be further improved by reducing the magnitude of the BICCs. This can be achieved by slowly increasing the average central field while an additional AC transport current causes a small AC field. The slowly increasing field will not cause significant losses and BICCs. The AC field causes the large \dot{B}_{ce} required for generating the power loss without provoking large BICCs as long as the period of the AC current is much smaller than the characteristic time of the BICCs.

8.5 Negative field-sweep rates

The maximum negative ramp rate in accelerator magnets is important since it determines the maximum possible de-excitation rate of the magnets if there is a quench in one of the series-connected magnets.

In this section the effect of the coupling currents and power loss on the maximum de-excitation rate is discussed. The very few results of quench currents, that are available on several 1 m long LHC dipole model magnets, are presented at the end of this section.

The RRL due to the IFCCs is not significantly influenced by the sign of the field-sweep rate, since the time constant τ_{if} is very small and the IFCCs almost immediately reach the steady-state value. The reduction of the quench current, as discussed in section 8.2.1, is about 0.1% (at the expected field-sweep rate $\dot{B}_{ce} = -0.084 \text{ Ts}^{-1}$), and is negligible compared to the available margin of at least 10% between operating current and critical current.

The effects of the ISCCs, the BICCs and the ISCL on the RRL is different for negative and positive \dot{B}_{ce} and are discussed in more detail.

ISCCs

If \dot{B}_{ce} is negative the transport current and the ISCCs have opposite sign near the aperture, where the field is maximum. This implies that the ISCCs cause a decrease of the strand current in the parts of the coil with the highest field, and hence they cause an *increase* of the margin of the coil (not taking into account the loss generated by the ISCCs). Only for very large negative \dot{B}_{ce} in combination with a very small R_c can the ISCCs cause a significant reduction of the quench current. However, these large field-sweep rates are not attained in accelerator magnets.

BICCs

The influence of the BICCs on the RRL is much smaller for negative \dot{B}_{ce} than positive \dot{B}_{ce} since the characteristic time τ_{bi} is large. This means that at the start of the de-excitation, when the field is high, the BICCs are still small. At increasing ramp time, the magnitude of the BICCs increases but the critical current $I_{C, str}$ also increases because the field decreases. Fig. 8.22 shows an example of the change in the strand currents as a function of the time during a linear de-excitation (in the case of the PBD magnet with $R_c = 1 \mu\Omega$, $\tau_{is} = 4 \text{ s}$, $C_{bi} = 2 \cdot 10^4 \text{ AsT}^{-1}$, $\tau_{bi} = 200 \text{ s}$, constant $T_b = 1.9 \text{ K}$).

At $t=0$ the strand current is about 30% smaller than the critical current which corresponds to an operation field of about 85% of B_q . The strand current increases because the increase of the current I_{bi} is larger than the decrease of the transport current $I_{tr, str}$. However, the strand will not quench since the critical current $I_{C, str}$ remains larger than I_{str} during the entire ramp. The magnitude of the BICCs is difficult to evaluate since the BICCs caused by the numerous non-uniformities in a coil partially cancel. This implies that the RRL due to the BICCs is difficult to estimate as well. An increase of R_a and R_c of the cable will definitely reduce the magnitude of the BICCs, but could, on the other hand, worsen the stability of the cable (see chapter 9). Hence, a certain optimum of R_a and R_c has to be found for which the BICCs are sufficiently small, without affecting the stability of the cable too much.

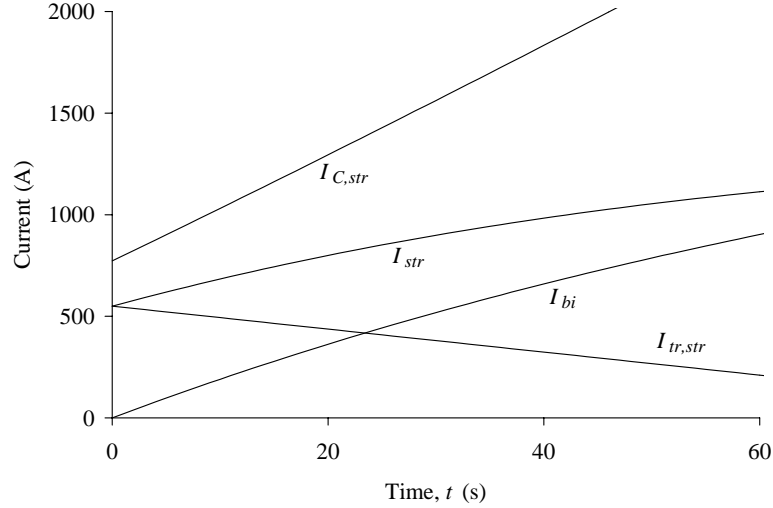


Figure 8.22. Simulation of the currents $I_{tr,str}$, $I_{C,str}$, I_{str} and I_{bi} during a ramp-down from 550 to 0 A in 100 s (only the first 60 s is shown). The BICC is assumed to be 0 at $t=0$. The increase of I_{bi} is larger than the decrease of the transport current. The critical current, however, increases still faster than the strand current and no quench will occur during the ramp-down.

It is preferable to investigate the effect of the BICCs experimentally by actually measuring the RRL of the magnet. Note that the magnitude of the BICCs could vary significantly among almost identical coils made of the same cable, due to small variations in the cable pitch and local R_a -, R_c - and ρ_s -distributions. The maximum de-excitation rate of a single magnet is therefore not representative for a series of magnets wound from the same cable. Hence, the RRL of several magnets has to be determined in order to be more or less sure that the BICCs will not cause a preliminary quench in any of the magnets of an accelerator ring during a fast de-excitation.

ISCL

The power loss caused by the coupling currents is independent of the sign of \dot{B}_{ce} . However, in the case of a negative \dot{B}_{ce} the time constant τ_{is} of the ISCCs implies that the ISCL will be relatively small during the first part of the ramp, where the difference between the currents $I_{C,str}$ and I_{str} is still small, and hence the temperature margin. A quench can only occur during the time that the temperature T_{cab} of the cable is still increasing (assuming constant BICCs). This is illustrated in Fig. 8.23 by means of a simulation of a fast de-excitation of the PBD magnet with $R_c=1 \mu\Omega$, $\tau_{is}=4$ s, $q=10^4 \text{ Wm}^{-3}\text{K}^{-1}$, $\dot{B}_{ce}=-0.1 \text{ Ts}^{-1}$, $C_{bi}=0$ and $T_b=1.9$ K. The temperature increase of the cable causes $I_{C,str}$ to decrease faster than $I_{tr,str}$. After about 6 s a quench occurs when $I_{tr,str}=I_{C,str}$.

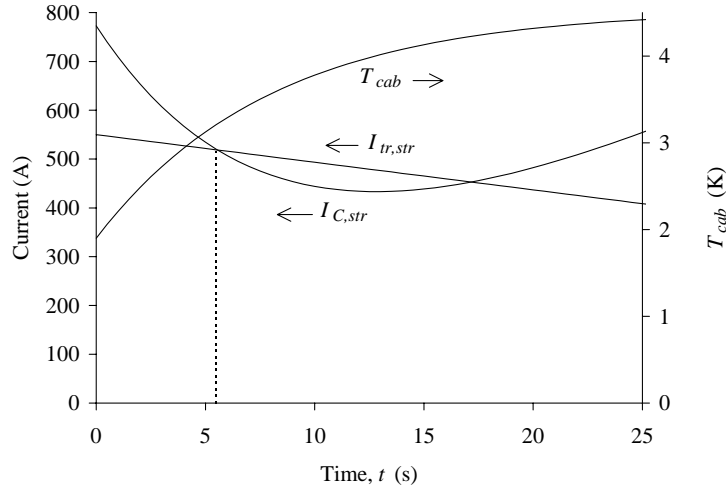


Figure 8.23. Simulation of the currents $I_{tr,str}$ and $I_{C,str}$ and the temperature T_{cab} during a linear ramp-down from 550 to 0 A in 100 s. A quench will occur at $t=6$ s where $I_{tr,str}=I_{C,str}$.

In practice, the time required for temperature stabilisation not only depends on the dissipation and the time constant τ_{is} but also on:

- the heat capacity of the cable and the helium which is present within the voids of the cable,
- the effective time constant of the heat transfer through the insulation. This time constant is estimated to be about 3–20 s for the LHC dipole model magnets and depends on the energy dissipation in the cable and the bath temperature [AT-MA, '93]. Figs. 8.15 and 8.16 indicate that complete temperature stabilisation takes about 100 s for field-sweep rates comparable to the initial de-excitation rate.

It is beyond the scope of this thesis to investigate the process of temperature stabilisation in a cable. In first approximation, it can be concluded that a quench due to the ISCL is likely to occur in the first 20 s of the de-excitation (for $R_c > 1 \mu\Omega$ so that $\tau_{is} < 5$ s). It is, however, possible that, due to a combination of the ISCL and the BICCs, a quench can occur after more than 20 s.

A few results of quenches on 1 m long LHC dipole model magnets are presented in Fig. 8.24, where the smallest (or critical) field-sweep rate $\dot{B}_{ce,cr}$ is shown at which a quench occurs as a function of the average R_c of the magnet. In all cases the de-excitation starts at an initial current equal to about $0.9I_{q,0}$. The quenches are performed using a constant field-sweep rate, instead of an exponentially decreasing one (with a time constant of about 100 s) as is the case during a fast de-excitation of the dipole magnets in LHC. This does, however, not affect $\dot{B}_{ce,cr}$, since all quenches occur during the first 15 s, which is much smaller than the de-excitation time constant.

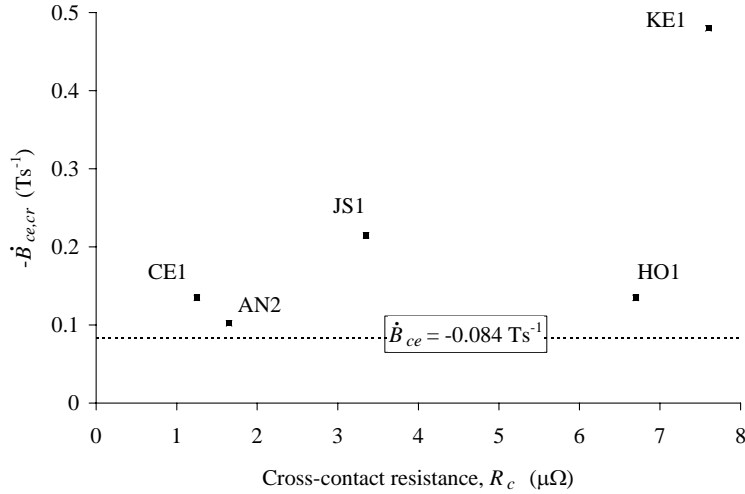


Figure 8.24. The critical de-excitation rate for a few LHC dipole model magnets. The fast de-excitation rate as anticipated for the LHC dipole magnets is shown by a dotted line.

The critical de-excitation rate of each magnet is larger than the anticipated fast de-excitation rate of LHC of about -0.084 Ts^{-1} . It is interesting to see that a correlation exists between the RRL for positive and negative \dot{B}_{ce} (see Figs. 8.12 and 8.24). This implies that probably also the AN1, EL1 and EL2 magnets, which exhibit a smaller RRL than the CE1 magnet can withstand negative field-sweep rates of at least -0.15 Ts^{-1} without quenching.

The number of magnets, of which $\dot{B}_{ce,cr}$ is measured, is still too small to draw a conclusion about the correlation between $\dot{B}_{ce,cr}$ and R_c . If $\dot{B}_{ce,cr}$ is only determined by the ISCL, a linear increase of $\dot{B}_{ce,cr}$ as a function of R_c is expected. In this case $\dot{B}_{ce,cr}$ of the HO1 magnet is much too small, which could be due to large BICCs or a small R_c locally in one of the turns. The fact that no clear correlation exists between $\dot{B}_{ce,cr}$ and R_c shows that a certain variation in $\dot{B}_{ce,cr}$ can be present for magnets with the same average R_c .

8.6 Conclusions

The ramp-rate limitation (RRL) of dipole magnets, and in particular LHC dipole magnets, is investigated as a function of the coupling currents and coupling loss in the cables. The presence of coupling currents and coupling loss always reduces the temperature margin of the coil during a ramp with positive field-sweep rate. Small transient heat pulses which would not lead to a quench under DC conditions could, therefore, provoke a quench while ramping the magnet. This stability effect is especially important in magnets for which the field-sweep rate is fixed. In accelerator magnets the field-sweep rate can often be reduced near the end of the excitation where the temperature margin is small.

The reduction of the quench current as a function of the ramp rate is very difficult to calculate since it is strongly dependent on the local variations in the heat dissipation and

cooling conditions. In addition, the process of current redistribution is unknown in case the strand currents locally exceed the critical current.

In general, the reduction of the quench current of accelerator magnets is not significantly affected by the interfilament coupling currents.

The shape of the $I_q-\dot{B}_{ce}$ curve between the quench current and the field-sweep rate shows whether the interstrand coupling currents (ISCCs), the boundary-induced coupling currents (BICCs) or the interstrand coupling loss (ISCL) are the main cause of the quench. The ISCCs result in a linear $I_q-\dot{B}_{ce}$ curve while the BICCs and the ISCL cause concave and convex shapes respectively.

Ramp-rate-induced quench experiments make it possible to estimate the magnitude of the BICCs and the increase of the cable temperature due to beam losses. For this purpose, the RRL of a few LHC dipole model magnets is evaluated at bath temperatures of 1.9 and 4.3 K.

The reduction of the quench current in the LHC dipole models at high ramp rates is mainly attributed to the interstrand coupling loss. The relative reduction of the quench current as a function of the ramp rate is about 50% larger at 4.3 K than at 1.9 K. All the quenches start in the inner coil near the midplane. At lower ramp rates, the reduction of the quench current caused by the BICCs can be significant. In the model magnets the magnitude of the BICCs is estimated to be about 30 A at 0.0066 Ts^{-1} (section 8.3) which corresponds to about the transport current in the strands at injection ($I_{tr,str} \approx 35 \text{ A}$) and about 7% of the transport current at nominal field ($I_{tr,str} \approx 470 \text{ A}$).

The temperature increase of the cable of the inner coil is estimated to be about $1.5 (\pm 0.5) \text{ K}$ for a heat dissipation of 10 mW/cm^3 (section 8.4). The cable temperature at smaller levels of dissipation could not be deduced. In the LHC magnets, beam losses will be present of up to 10 mW/cm^3 . The temperature increase will then be too large to ensure a proper performance of the magnets. A temperature increase smaller than 0.25 K is required in order to keep the coils at a temperature below the lambda temperature and benefit from the good thermal properties of superfluid helium. Hence, either the porosity of the cable insulation or the beam shield has to be improved.

The maximum de-excitation rate of a magnet has to be determined experimentally since calculations are too speculative. Several magnets have to be investigated to be sure that variations in the cooling, heat dissipation and BICCs, which are likely to be present, even in identical magnets made of the same cable, will not cause a preliminary quench during a fast de-excitation. The RRL of the LHC dipole model magnets for positive and negative field-sweep rates \dot{B}_{ce} seem to be correlated. A large RRL for positive \dot{B}_{ce} implies a large RRL for negative \dot{B}_{ce} . All the model magnets can probably be discharged with a field-sweep rate of -0.084 Ts^{-1} (as anticipated for a fast de-excitation of the LHC magnets) without quenching. Quench experiments on more model magnets are required to draw specific conclusions concerning the correlation between the maximum de-excitation rate and R_c . A good understanding of this correlation is necessary to specify the contact resistance for accelerator magnets.